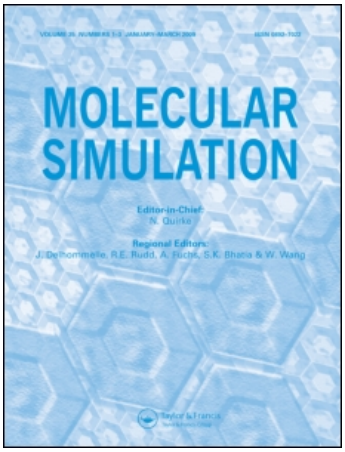

Molecular Simulation
Publication details, including instructions for authors and subscription information:
http://www.informaworld.com/smpp/title~content=t713644482

Molecular dynamics simulation of water confined in a nanopore of amorphous silica

Qingyin Zhang[a]; Kwong-Yu Chan[a]; Nicholas Quirke[b]
[a] Department of Chemistry, The University of Hong Kong, Hong Kong, P.R. China [b] Department of Chemistry, Imperial College of Science, Technology, and Medicine, London, UK

To cite this Article Zhang, Qingyin , Chan, Kwong-Yu and Quirke, Nicholas(2009) 'Molecular dynamics simulation of water confined in a nanopore of amorphous silica', Molecular Simulation, 35: 15, 1215 — 1223
To link to this Article: DOI: 10.1080/08927020903116029
URL: http://dx.doi.org/10.1080/08927020903116029

Molecular Simulation
Vol. 35, No. 15, December 2009, 1215–1223

Taylor & Francis
Taylor & Francis Group

Molecular dynamics simulation of water confined in a nanopore of amorphous silica

Qingyin Zhang[a], Kwong-Yu Chan[a]* and Nicholas Quirke[b]

[a]*Department of Chemistry, The University of Hong Kong, Pokfulam Road, Hong Kong, P.R. China;* [b]*Department of Chemistry, Imperial College of Science, Technology, and Medicine, London, UK*

(*Received 24 February 2009; final version received 12 June 2009*)

Molecular dynamics simulations are performed to study the transport and structural properties of water confined in a cylindrical silica nanopore. The pore wall is amorphous and mimics a typical mesoporous silica material. The diameters of silica pores studied are 4.75, 9.51, 20 and 25 Å. The self-diffusion of water calculated decreases with pore size and indicates much slower transport compared to the bulk phase. Strong adsorption of water to the silica wall is observed in the density profiles, indicating the hydrophilic nature of the wall. The hydrogen-bonding network is strongly affected by water–silica wall interaction. The average number of hydrogen bonds per water decreased with decreasing pore diameter.

Keywords: silica nanopore; confined water; amorphous silica

1. Introduction

The study of confined liquids by molecular dynamics has led to the understanding of fascinating adsorption, phase transition and transport phenomena [1–4]. In recent years, molecular simulation studies have focused more on real materials with structured surfaces such as carbon nanotubes [5–7], activated carbon nanofibres [8,9], molecular sieves [10] and porous glass [11]. The class of ordered mesoporous silicas, first reported for MCM-41 [12], has now become a widely used platform for studying catalysis [13,14], separation technologies [15] and behaviour of confined liquids [16]. To complement and guide experiments, it will be necessary to perform molecular simulation studies of a liquid confined in mesoporous silica and water is the obvious choice of liquid to study. The strong water–silica wall interaction together with the exclusion effect of confinement will lead to large deviation of bulk behaviour. Lee and Rossky [17] reported molecular dynamics simulations of liquid water at silica surface with terminal functional group adapted to be either hydrophobic or hydrophilic. The results showed that hydrophobicity destroys the hydrogen-bonding network of water near the interface. Brodka and Zerka [18] proposed later an amorphous silica pore model. Gallo and co-workers studied TIP4P water confined in a 40 Å silica pore [19] and SPC/E water confined in cylindrical silica pores or glass pores [20–32]. In these works, transport and structural analysis of water confined in a 40 Å silica pore at room temperature are reported. Liu et al. [33] used molecular dynamics to study the dynamics of super-cooled water confined in a silica pore. Giovambattista et al. [34] studied the phase transition of water confined between two silica plates under different pressures. The empirical potential model proposed by Brodka and Zerda [18] consisted of the (12-6) Lennard-Jones (LJ) and Coulomb interactions but the adopted model does not maintain charge neutrality of the silica nanopore and the LJ parameters of Si are unrealistically set to zero. Furthermore, to the best of our knowledge, there is no report on water confined in a very small silica pore, when the pore diameter is only one and a half to three times the water molecule. We report here molecular dynamics simulations of water confined in silica nanopores of different diameters with an improved potential model to investigate the transport and structure properties of severely confined water.

2. Simulation details

Figure 1 illustrates the cylindrical silica nanopore created by removing atoms in a cylindrical region of an amorphous silica structure. The amorphous structure was created by heating crystalline silica to melting and followed by cooling without sufficient time for crystallisation. The amorphous configuration is the same as that constructed in [35] and the procedure of creating the silica nanopore is similar to the method used in Brodka and Zerda [18]. The length of the periodic simulation box is 35.83 Å. All atoms lying along the z-axis within a radius $d/2$ were removed, where d is the diameter of the pore. The oxygen atom bonded with two adjacent silicon atoms was the bridging oxygen. The oxygen bonded with only one silicon atom was the non-bridging oxygen. At the surface region of the pore wall (dark grey area in Figure 1), all silicon atoms that were bonded to less than

*Corresponding author. Email: hrsccky@hku.hk

ISSN 0892-7022 print/ISSN 1029-0435 online

DOI: 10.1080/08927020903116029
http://www.informaworld.com

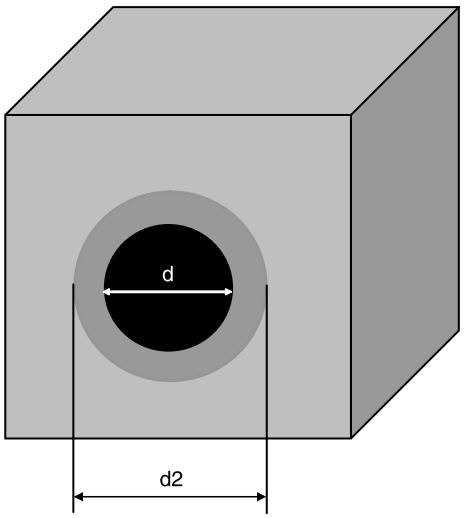

Figure 1. Schematic of the silica nanopore construction.

four oxygen atoms and silicon atoms bonded to three non-bridging oxygen atoms were removed. All non-bridging oxygen atoms with a dangling free bond were saturated with hydrogen atoms. The length of O—H bond was 0.1 nm and the angle of Si—O—H was 116°. During simulation, all atoms in the silica wall were frozen. Four different sizes of silica pore were constructed by the same procedure, with diameters d at 4.75, 9.51, 20.0 and 25.0 Å. The density of water confined in the silica pore cannot be undisputedly determined for the irregular pore wall. Here, the diameter d was used to calculate the volume of silica pore and the density of water confined in a silica pore. The densities of water confined in a silica pore were set to 0.9 and 1.0 g/cm^3 for four different silica pores. Equilibrium molecular dynamics (EMD) simulations were performed in a canonical or closed isochoric isothermal (NVT) ensemble at 298.15 K with a Gaussian thermostat. The time step was 1 fs. For 4.75 and 9.51 Å silica pores, the pore volumes in a cubic box were too small to hold several hundreds of water molecules. Therefore, the pore structures were duplicated in z directions by extended images. The final lengths of the 4.75 and 9.51 Å pores were 107.49 and 358.3 Å, respectively. Details of the silica pore geometry and simulations are listed in Table 3.

There are two main interactions in the simulations. They are water–water interactions and water–silica wall interactions. Both interactions contain the LJ term and Coulombic term. The interaction of water–water and water–wall can be expressed by

$$u_{\alpha\beta}(r_{ij}) = 4\varepsilon_{\alpha\beta}\left[\left(\frac{\delta_{\alpha\beta}}{r_{ij}}\right)^{12} - \left(\frac{\delta_{\alpha\beta}}{r_{ij}}\right)^{6}\right] + \frac{q_i q_j}{4\pi\varepsilon_0 r_{ij}}, \quad (1)$$

where q_i is the charge of one site, r_{ij} is distance between two sites of molecules. The interaction terms $\varepsilon_{\alpha\beta}$ and $\delta_{\alpha\beta}$ can be calculated by the Lorentz–Berthelot mixing rules

$$\varepsilon_{\alpha\beta} = \sqrt{\varepsilon_\alpha \varepsilon_\beta}, \quad (2a)$$

and

$$\delta_{\alpha\beta} = \frac{\delta_\alpha + \delta_\beta}{2}, \quad (2b)$$

where $\varepsilon_{\alpha\beta}$ and $\delta_{\alpha\beta}$ are the LJ interaction parameters between α and β sites.

The original empirical potential model proposed by Brodka and Zerda [18] consisted of the (12-6) LJ and Coulomb interactions and the parameters are listed in Table 1. The model used in Brodka and Zerda [18] cannot maintain charge neutrality of the silica nanopore and LJ parameters of Si are unrealistically set to zero. Modifications are, therefore needed. At the silica pore wall, there are three types of silicon considering the neighbours as follows:

(1) One silicon atom connected with four bridged oxygen atoms.
(2) One silicon atom connected with three bridged oxygen atoms and one non-bridged oxygen (nbO) atom.
(3) One silicon atom connected with two bridged oxygen (bO) atoms and two nbO atoms.

The total net charge of silica pore can be calculated in each case. For example, in case 1, the total charge is $q_{Si} + 4 \times q_{bO}/2 = +1.283 + 4(-0.629)/2 = +0.025$. In cases 2 and 3, the total net charges are +0.0125 and 0, respectively. So the charge parameters used in Brodka

Table 1. Potential parameters in Brodka and Zerda [18] and those modified in this study.

	σ (nm)		ε (kJ/mol)		q (e)	
	Ref [2]	This work	Ref [2]	This work	Ref [2]	This work
bO	0.270	0.270	1.912	1.912	−0.629	−0.6415
nbO	0.300	0.300	1.912	1.912	−0.533	−0.52675
Si	0	0.3795	0	0.5336	+1.283	+1.283
H	0	0	0	0	+0.206	+0.206

bO, Bridged oxygen connected to two silicon atoms and nbO, non-bridged oxygen connected to one silicon atom and one hydrogen atom.

Table 2. Potential parameters of the SPC/E model.

	σ (nm)	ε (kJ/mol)	q (e)
O	0.3169	0.6502	−0.8476
H	0	0	+0.4238

and Zerda potential cannot maintain neutralisation of the simulation system. The charges of bridged oxygen and nbO are therefore adjusted with the new values listed in Table 1. Using the new parameters, the net charges of three cases are all equal to zero. Furthermore, in Brodka and Zerda's original model, the volume and energy parameters of LJ for Si atoms are all equal to zero. This is not realistic in a silica pore. We therefore modified the LJ parameters of silicon according to the potential parameters used in [17].

The water molecules are modelled by the SPC/E potential [36] which has positive partial charges on H atoms and a negative partial charge plus an LJ interaction on the O atom located at the centre of the molecule. The distance between H and O atoms is 1 Å and the bond angle of H—O—H is 109°47′. The potential parameters are listed in Table 2.

The long-range Coulomb force was calculated by the 'charge line' method [37]. This method was successfully applied in previous molecular simulations with a cylindrical structure and the corresponding interaction terms are

$$U_{ij} = \frac{q_i q_j}{4\pi\varepsilon_0}\left(\frac{1}{r_{ij}} + \frac{1}{\sqrt{x_{ij}^2+y_{ij}^2+(H+z_{ij})^2}} + \frac{1}{\sqrt{x_{ij}^2+y_{ij}^2+(H-z_{ij})^2}}\right) + \frac{q_i q_j}{4\pi\varepsilon_0}\left[\begin{array}{l}\ln\left(3H/2 - z_{ij} + \sqrt{x_{ij}^2+y_{ij}^2+(3H/2-z_{ij})^2}\right) \\ +\ln\left(3H/2 + z_{ij} + \sqrt{x_{ij}^2+y_{ij}^2+(3H/2+z_{ij})^2}\right)\end{array}\right], \quad (3)$$

where q_i is the charge of ion i, H is the length of cylindrical pore, ε_0 is the permeability in free space and z_i is the axial coordinate.

We consider that the diffusion is anisotropic and only the component along z direction is considered. So the Einstein relation can be expressed as

$$B + 2Dt = \frac{1}{N}\sum_{i=1}^{N}\left\langle \left|\mathbf{r}_{i,z}(t_0+t) - \mathbf{r}_{i,z}(t_0)\right|^2 \right\rangle, \quad (4)$$

where D is self-diffusion coefficient, $\mathbf{r}_n(t)$ is the position vector of the nth oxygen ion at time t and B is a constant.

3. Results and discussion

3.1 Density profiles of water

Figure 2(a) shows the radial density profiles of oxygen and hydrogen atoms of water in a 4.75 Å silica nanopore. When $r = 0$, the atom locates at the centre of pore. The vertical axis represents the reduced density of hydrogen or oxygen atoms. From the plot, the density of oxygen decreases with increasing r. This implies that most of the water molecules are located at the centre of the pore. The density profile of hydrogen has the same character as the oxygen curve except at the centre region of the pore, because the positions of oxygen and hydrogen cannot overlap. Comparing the density profiles of two species at the region near the silica wall, the hydrogen atoms approach the wall more closer than the oxygen atoms. This implies that the structure of water near the wall is dominated by nbO and hydrogen atoms in the silica wall.

Figure 2(b) shows the density profiles of water confined in 9.51 Å. Different from 4.75 Å pore, the maximum density of water is not located at the centre of the pore. The peak is located at $r = 3$ Å. Most of the water molecules are likely to be distributed in the region between the centre and wall of the 9.51 Å pore. In the density profiles of two densities, there are two main differences. One is that the maximum peak of high density is higher than that of low density. The other is the density in the central region of pore. The density profile of central region of $\rho = 1.0\,\mathrm{g/cm^3}$ is obviously higher than the same region of $\rho = 0.9\,\mathrm{g/cm^3}$.

Figure 2(c) shows the density profiles of water confined in a 20 Å silica. Quite different from the cases of smaller pores, there are three shells of water in a silica pore.

Table 3. Set-up of simulations.

d Å	ρ (g/cm^3)	Number of Si	Number of bO	Number of nbO	Number of H	Number of H_2O	Simulation run time (ns)
4.75	0.9	9700	19100	600	600	190	0.5
9.51	0.9	2724	5298	300	300	228	1
9.51	1.0	2724	5298	300	300	255	1
20.0	0.9	663	1236	180	180	338	1
20.0	1.0	663	1236	180	180	376	1
25.0	0.9	510	910	220	220	528	1
25.0	1.0	510	910	220	220	588	1

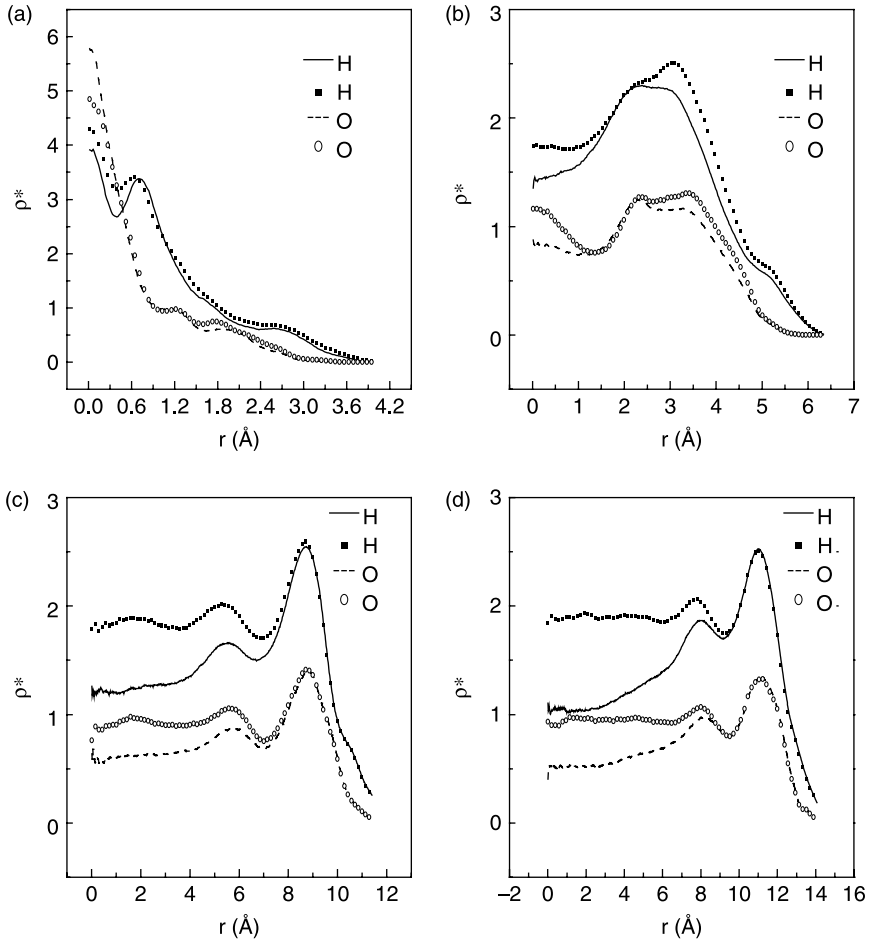

Figure 2. Density profiles of water confined in a silica nanopore. (a) $d = 4.75$ Å; (b) $d = 9.51$ Å; (c) $d = 20$ Å; (d) $d = 25$ Å. Lines: $\rho = 0.9\,\mathrm{g/cm^3}$. Symbols: $\rho = 1.0\,\mathrm{g/cm^3}$.

The density at the wall is much higher than the bulk density of water due to the strong attraction of the silica wall. The main difference of the two profiles in Figure 2(c) is the density of inner layer water. The density of inner layer water at $\rho = 1.0\,\mathrm{g/cm^3}$ is expectedly higher than that of $\rho = 0.9\,\mathrm{g/cm^3}$. The density profiles showing the hydrophilic character of the larger nanopores are consistent with previous simulation results [41]. Figure 2(d) shows the density profiles of water confined in a 25 Å pore with features same as those in Figure 2(c).

3.2 Self-diffusion of water

Figure 3(a) shows a typical mean square displacement (MSD) curve of a 4.75 Å silica nanopore. Multiple time origins method was used in the calculation of the MSD curve. Because the silica pore is a cylindrical structure, only diffusion in z-axis is considered. Linear fitting the MSD curve, the self-diffusion coefficients of water can be obtained by Equation (4). The calculated average self-diffusion coefficient of water is $4.8 \times 10^{-11}\,\mathrm{m^2/s}$, which is one 1/40 that of the value in SPC/E bulk water [38,39] and experimental data [40] of bulk water at room temperature. Two factors lead to the very slow diffusion observed. One is the serious confinement effect on water. The diameter of the pore is 4.75 Å whereas the diameter of SPC/E water is 3.169 Å. The water molecules form a single file in the silica pore. The other factor is the strong interaction between water and silica wall leading to friction.

Figure 3(b) shows the typical MSD curves of water confined in larger silica nanopores. The density of water is $0.9\,\mathrm{g/cm^3}$. When $d = 9.51$ Å, the diffusions of water are faster than in the case of a 4.75 Å pore. At this pore size, the denser fluid has lower diffusion coefficients. When $d = 20$ or 25 Å, the diffusion coefficients of water are similar. These values are still lower than that of the bulk water. Comparing the diffusion coefficients at the two densities in 20 and 25 Å pores, there is no distinct difference between them. When a fluid is confined in a cylindrical pore, the density distribution of the fluid can affect the overall diffusion coefficients. The fluid layer

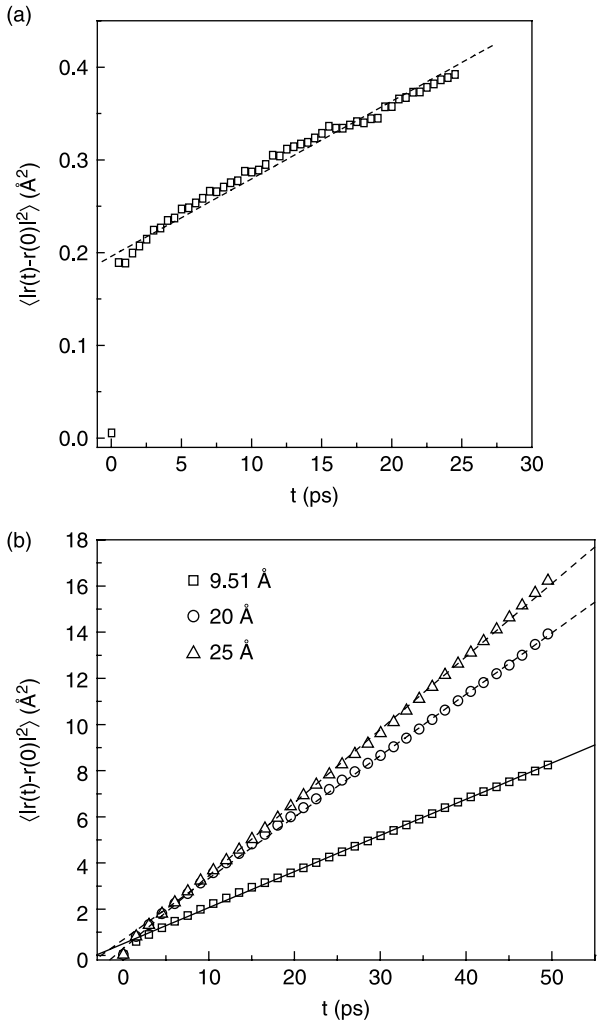

Figure 3. MSD curve of water confined in a silica nanopore. (a) $d = 4.75$ Å; and (b) $d = 9.51$, 20, 25 Å, $\rho = 0.9\,\mathrm{g/cm^3}$.

close to the wall has a lower diffusion and the fluid layer located at the centre of pore has a larger diffusion [18]. These are shown in Figure 4. When confined in a silica nanopore, water molecules prefer to locate near the wall due to the hydrophilic property of wall. Figure 5 shows the change of diffusion coefficients of water confined in a silica nanopore of different pore diameters. With increasing diameter, the self-diffusion coefficient increases at both densities. The self-diffusion coefficients of water confined in a 40 Å vycor glass pore [21] are shown in Figure 5. To extrapolate our simulation results to 40 Å, it is in agreement with the diffusion coefficients of water in [21].

3.3 Radial distribution functions of water confined in silica pores

Figure 6 shows the radial distribution functions of water confined in four silica nanopores. The radius distribution

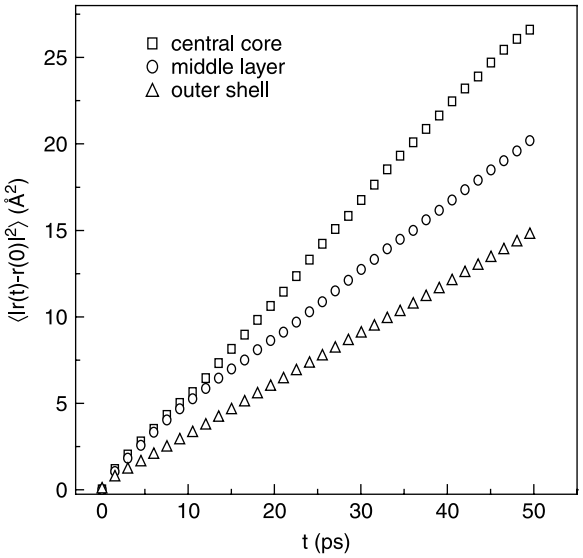

Figure 4. MSDs of water confined in different shells in a 25 Å silica nanopore at $\rho = 0.9\,\mathrm{g/cm^3}$.

functions can be calculated by

$$g_{\alpha\beta}(r) = \frac{\overline{n}^2_{\alpha\beta}(r)}{(N_\beta/V)\delta V(r)}, \tag{5}$$

where $\overline{n}^2_{\alpha\beta}(r)$ is the average site–site pairs inside a spherical shell $\delta V(r)$, N_β is the number of type β.

The lines are results of $\rho = 0.9\,\mathrm{g/cm^3}$ and the symbols are results of $\rho = 1.0\,\mathrm{g/cm^3}$. The difference between the two densities is small, the first peak of H—H, O—H and O—O at low density is slightly shifted to right compared

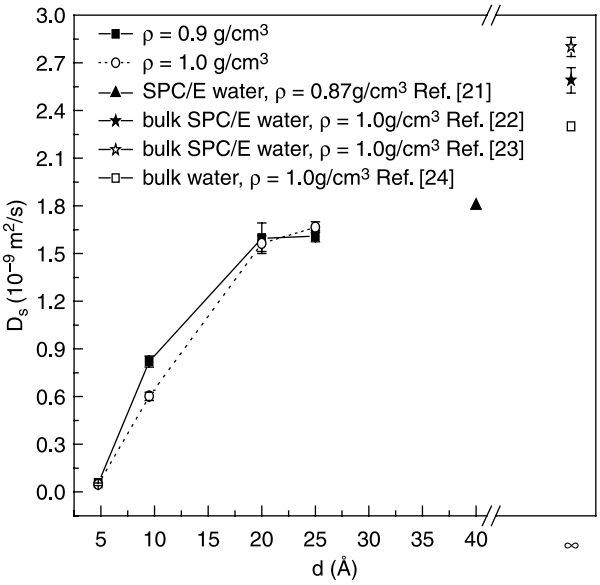

Figure 5. Diffusion coefficient of water confined in silica nanopores of different sizes.

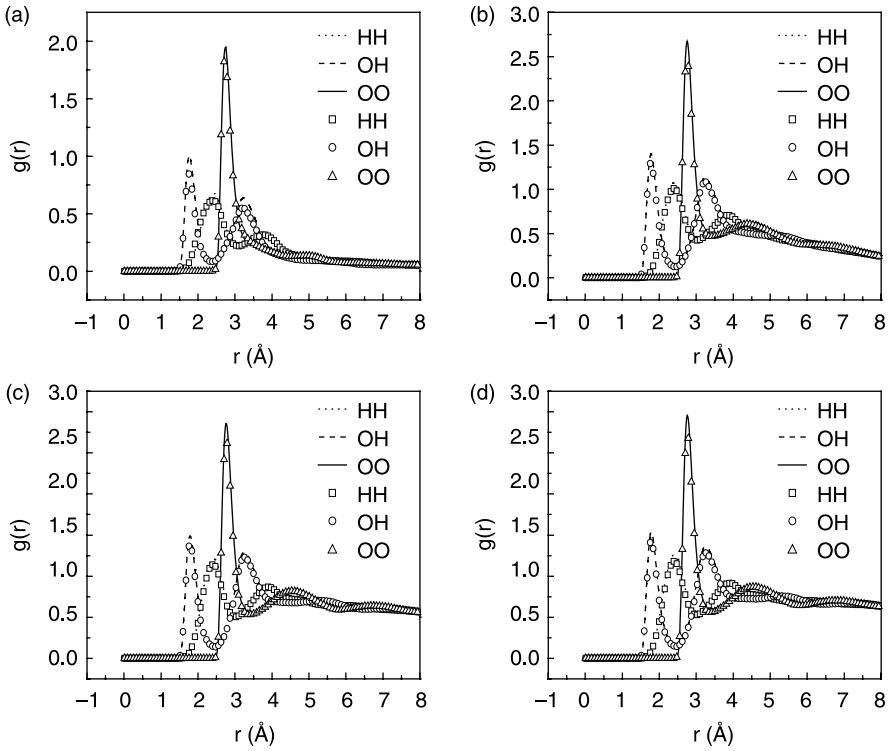

Figure 6. Radial distribution curves of water confined in a silica nanopore. (a) $d = 4.75$ Å; (b) $d = 9.51$ Å; (c) $d = 20$ Å; (d) $d = 25$ Å. Lines: $\rho = 0.9\,\mathrm{g/cm^3}$. Symbols: $\rho = 1.0\,\mathrm{g/cm^3}$.

with the results of high density, and the amplitudes of these peaks are also slightly higher than those of high density. These phenomena are similar to Parker's results [41]. When density is low, there is enough space for water to form a hydrogen network. The water molecules may form more clusters than at high density. In Figure 6, the long range $g(r)$ deviates from 1.0 at large r due to the confined geometry.

3.4 Site–site distribution functions of water and silica wall

Figure 7 shows the site–site distribution curves of silica wall and water. The site–site distribution function can be expressed by

$$\rho_{\alpha\beta}(r) = \frac{\overline{n}^2_{\alpha\beta}(r)}{\delta V(r)}, \tag{6}$$

where $\overline{n}^2_{\alpha\beta}(r)$ is the average site pairs inside a spherical shell $\delta V(r)$, N_β is the number of type β.

From these figures, the H and nbO attach to the H site of SPC/E water more closely than the O site of SPC/E. Comparing the amplitude of first peaks with the same pore diameter but different densities. In Figure 7(b), the amplitude of the first peak at high density in 9.51 Å pore is higher than that of low density. This relates to the density profiles of 9.51 Å pore (Figure 2(b)). The maximum of density occurs at $r = 3$ Å at two densities. The distance between the position of highest peak and wall is about 3 Å. The value is close to the first peak position of nbO—O curves in Figure 7(b). In Figure 2(b), the amplitude of high density is higher than that of low density. So, in Figure 7(b), the amplitude of first peak at high density is higher than that of low density. However, in Figure 7(c) and (d), the amplitude of first peaks at low density is slightly higher than that of high density and this trend is reversed at the second peaks of pair correlation curves. This also can be illustrated by the density profiles in Figure 2(c) and (d). In the cases of 20 and 25 Å pores, though the overall densities of water are different, the partial densities near the silica wall are nearly the same. The amplitudes of first peaks at the two densities are nearly the same. The high amplitude at low density might be a statistical error or the water at low density can form a more stable and close structure with the silica wall.

3.5 Hydrogen bond network of water confined in silica pores

A geometrical definition was used to count the numbers of hydrogen bond. Two water molecules are hydrogen bonded when these three conditions are satisfied [42]: $R_{\mathrm{O—O}} < 3.75$, $R_{\mathrm{O—H}} < 2.46$ Å and $\angle \mathrm{OO}\ldots\mathrm{OH} < 30°$.

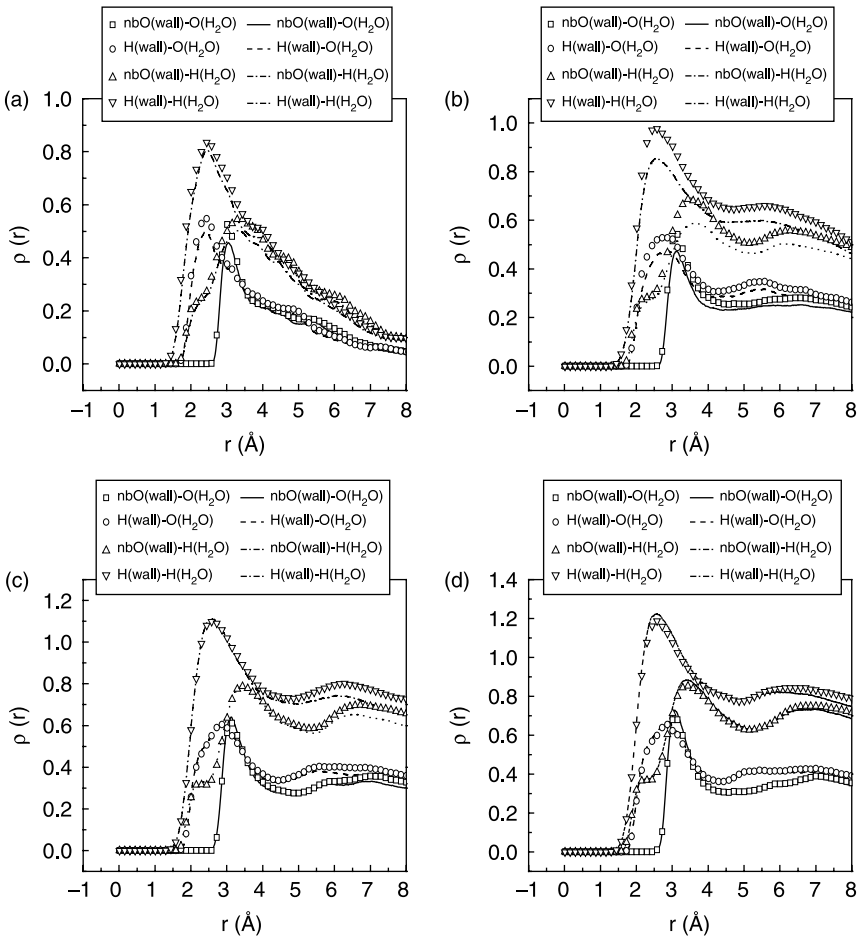

Figure 7. Site–site distribution functions of water and silica wall in a silica nanopore. (a) $d = 4.75$ Å; (b) $d = 9.51$ Å; (c) $d = 20$ Å; (d) $d = 25$ Å. Lines: $\rho = 0.9\,\mathrm{g/cm^3}$. Symbols: $\rho = 1.0\,\mathrm{g/cm^3}$.

Figure 8 shows the average number of hydrogen bonds of a water molecule located at various radial positions. In bulk liquid water, each molecule forms on average four hydrogen bonds either as O—H or H—O [43]. In Figure 8(a), due to the severe confinement and attraction with silica wall, the average number of hydrogen bonds was reduced, particularly for the case of 4.75 Å. Even in the centre of the 4.75 Å pore, the average number of hydrogen bond is only about one half that of bulk water. There is no flat region in H bonding distribution case and the average number of hydrogen bond drops towards the wall. In the 9.51 Å silica pore, a short flat region can be observed. It is closer to the H bond number in bulk water though the value is still lower than that of bulk water. Both curves in Figure 8(b) begin to drop at $r = 2$ Å. The distance between this point and the edge of pore is about 4 Å and it matches the diameter of water. In Figure 8(c) and (d), a broader 'flatten' region can be observed in the relative large pores and the curves of high densities show higher intensities and the dropping regions are all about 4 Å. It is interesting to notice that the curves of different densities show quite similar behaviour near the wall. It reveals that water can form similar hydrogen bond networks in the depletion region at the wall with different densities. In all cases, the average number of hydrogen bond corresponding to the bulk water is lower than that of bulk water. So the confined and interaction between water and silica wall can frustrate the water–water hydrogen bond network in a silica pore. Also shown in Figure 8 is the breakdown into the number of water–water and water–wall H bonds. Water–wall bonding can be between H of water and O of silica or O of water and H of bridged O. Near the wall, H bond between water and wall increases, replacing many water–water bonding.

4. Conclusions

EMD simulations are employed to study the transport properties and structural properties of SPC/E water confined in a cylindrical silica nanopore. Through simulations, the self-diffusion coefficients of water confined in 4.75, 9.51, 20 and 25 Å are calculated.

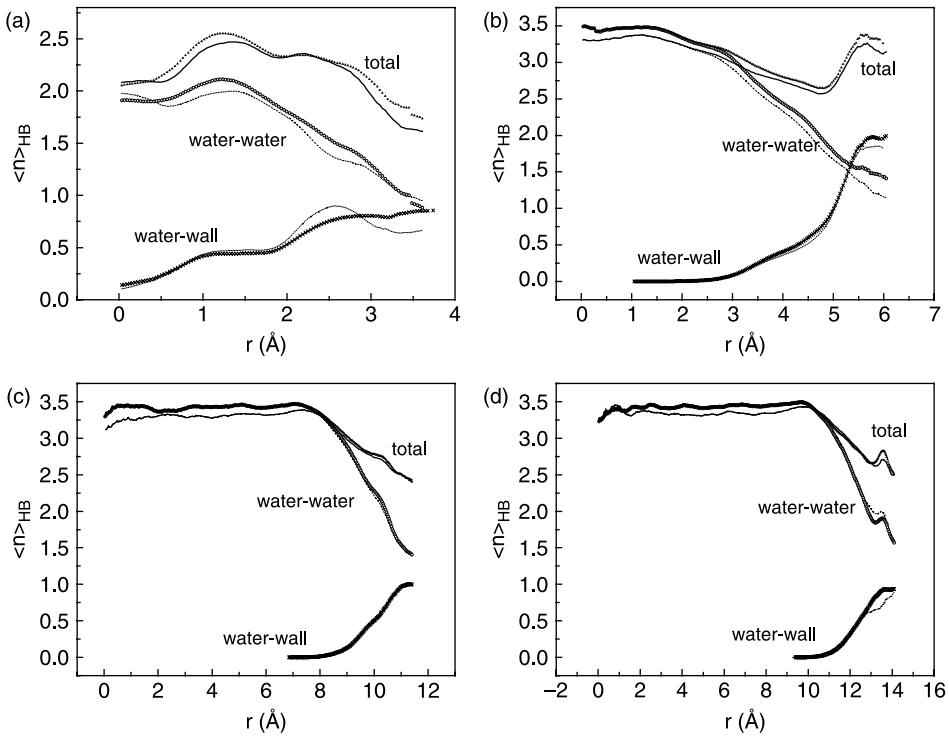

Figure 8. Number of hydrogen bonds per water molecule confined in a silica nanopore. [Lines $\rho = 0.9\,\mathrm{g/cm^3}$ dashed line: water–water H bond, dotted line: water–wall H Bond, solid line: total H bond; Symbols $\rho = 1.0\,\mathrm{g/cm^3}$: open circles: water–water H bond, crosses: water–wall H-Bond, solid triangles: total H-bond] (a) $d = 4.75$ Å; (b) $d = 9.51$ Å; (c) $d = 20$ Å; (d) $d = 25$ Å.

Due to the severe confinement effect, the diffusion in a silica pore is slower than that of bulk water at room temperature. The diffusion coefficient increases with increasing pore sizes. From the structure analyses, the diameters of silica pore affect the density profiles of water. In 4.75 Å pores, due to severe confinement effect, the water molecules locate at the centres of pore. In larges pores, 20 and 25 Å, the water molecules prefer to locate at the surface of wall. This reveals the nature of a hydrophilic wall. The density profiles of water in 9.51 Å pore reveal a competing relationship between severe confinement and hydrophilic nature of silica wall. Through the analysis of average number of hydrogen bonds, the hydrogen network of water–water was shown to be broken by the confinement and interaction of silica wall.

Acknowledgement

This research was supported by the General Research Fund (HKU 7006/05P).

References

[1] L.D. Gelb, K.E. Gubbins, R. Radhakrishnan, and M. Sliwinska-Bartkowiak, *Phase separation in confined systems*, Rep. Prog. Phys. 62(12) (1999), pp. 1573–1659.

[2] M. Alcoutlabi and G.B. McKenna, *Effects of confinement on material behaviour at the nanometre size scale*, J. Phys.: Condens. Matter 17(15) (2005), pp. R461–R524.

[3] C. Alba-Simionesco, B. Coasne, G. Dosseh, G. Dudziak, K.E. Gubbins, R. Radhakrishnan, and M. Sliwinska-Bartkowiak, *Effects of confinement on freezing and melting*, J. Phys.: Condens. Matter 18(6) (2006), pp. R15–R68.

[4] L.A. Pozhar, *Structure and dynamics of nanofluids: theory and simulations to calculate viscosity*, Phys. Rev. E 61(2) (2000), pp. 1432–1446.

[5] R.E. Tuzun, D.W. Noid, B.G. Sumpter, and R.C. Merkle, *Dynamics of fluid flow inside carbon nanotubes*, Nanotechnology 7(3) (1996), pp. 241–246.

[6] Z.G. Mao and S.B. Sinnott, *Predictions of a spiral diffusion path for nonspherical organic molecules in carbon nanotubes*, Phys. Rev. Lett. 89(27) (2002), 278301-1–278301-4.

[7] A.I. Skoulidas, D.M. Ackerman, J.K. Johnson, and D.S. Sholl, *Rapid transport of gases in carbon nanotubes*, Phys. Rev. Lett. 89(18) (2002), 185901-1–185901-4.

[8] M. Sliwinska-Bartkowiak, R. Radhakrishnan, and K.E. Gubbins, *Effect of confinement on melting in slit-shaped pores: experimental and simulation study of aniline in activated carbon fibers*, Mol. Simul. 27(5–6) (2001), pp. 323–337.

[9] A. Striolo, K.E. Gubbins, M.S. Gruszkiewicz, D.R. Cole, J.M. Simonson, and A.A. Chialvo, *Effect of temperature on the adsorption of water in porous carbons*, Langmuir 21(21) (2005), pp. 9457–9467.

[10] M.G. Ahunbay, *Molecular simulation of adsorption and diffusion of chlorinated alkenes in ZSM-5 zeolites*, J. Chem. Phys. 127(4) (2007), 044707-1–044707-6.

[11] L.D. Gelb and K.E. Gubbins, *Characterization of porous glasses: simulation models, adsorption isotherms, and the Brunauer–Emmett–Teller analysis method*, Langmuir 14(8) (1998), pp. 2097–2111.

[12] J.S. Beck, J.C. Vartuli, W.J. Roth, M.E. Leonowicz, C.T. Kresge, K.D. Schmitt, C.T.W. Chu, D.H. Olson, E.W. Sheppard, S.B. Mccullen, J.B. Higgins, and J.L. Schlenker, *A new family of mesoporous molecular-sieves prepared with liquid-crystal templates*, J. Am. Chem. Soc. 114(27) (1992), pp. 10834–10843.

[13] G. Gerstberger and R. Anwander, *Screening of rare earth metal grafted MCM-41 silica for asymmetric catalysis*, Microporous Mesoporous Mater. 44 (2001), pp. 303–310.
[14] K. Yamamoto, Y. Nohara, and T. Tatsumi, *Synthesis and catalysis of Ti-MCM-41 materials with organic–inorganic hybrid network*, Chem. Lett. 30 (2001), pp. 648–649.
[15] T. Sano, K. Doi, H. Hagimoto, Z. Wang, T. Uozumi, and K. Soga, *Adsorptive separation of methylalumoxane by mesoporous molecular sieve MCM-41*, Chem. Commun. (1999), pp. 733–734.
[16] C. Mondelli, M.A. Gonzalez, F. Albergamo, C. Carbajo, M.J. Torralvo, E. Enciso, F.J. Bermejo, R. Fernandez-Perea, C. Cabrillo, V. Leon, and M.L. Saboungi, *Collective excitations in liquid D-2 confined within the mesoscopic pores of a MCM-41 molecular sieve*, Phys. Rev. B 73 (2006), 094206.
[17] S.H. Lee and P.J. Rossky, *A comparison of the structure and dynamics of liquid water at hydrophobic and hydrophilic surfaces – a molecular-dynamics simulation study*, J. Chem. Phys. 100(4) (1994), pp. 3334–3345.
[18] A. Brodka and T.W. Zerda, *Dynamics of liquid acetone: computer simulation*, J. Chem. Phys. 104(16) (1996), pp. 6313–6318.
[19] M. Rovere, M.A. Ricci, D. Vellati, and F. Bruni, *A molecular dynamics simulation of water confined in a cylindrical SiO_2 pore*, J. Chem. Phys. 108(23) (1998), pp. 9859–9867.
[20] P. Gallo, M. Rovere, M.A. Ricci, C. Hartnig, and E. Spohr, *Evidence of glassy behaviour of water molecules in confined states*, Phil. Mag. B, J. Phys. Condens. Matter Statis. Mech. Elect. Opt. Magn. Prop. 79(11–12) (1999), pp. 1923–1930.
[21] E. Spohr, C. Hartnig, P. Gallo, and M. Rovere, *Water in porous glasses a computer simulation study*, J. Mol. Liq. 80(2–3) (1999), pp. 165–178.
[22] P. Gallo and M. Rovere, *Molecular dynamics study of the glass transition in confined water*, J. Phys. 10(P7) (2000), pp. 203–206.
[23] P. Gallo, M. Rovere, M.A. Ricci, C. Hartnig, and E. Spohr, *Non-exponential kinetic behaviour of confined water*, Europhys. Lett. 49(2) (2000), pp. 183–188.
[24] P. Gallo, M. Rovere, and E. Spohr, *Supercooled confined water and the mode coupling crossover temperature*, Phys. Rev. Lett. 85(20) (2000), pp. 4317–4320.
[25] P. Gallo, M. Rovere, and E. Spohr, *Glass transition and layering effects in confined water: a computer simulation study*, J. Chem. Phys. 113(24) (2000), pp. 11324–11335.
[26] C. Hartnig, W. Witschel, E. Spohr, P. Gallo, A. Ricci, and M. Rovere, *Modifications of the hydrogen bond network of liquid water in a cylindrical SiO_2 pore*, J. Mol. Liq. 85(1–2) (2000), pp. 127–137.
[27] P. Gallo, M. Rapinesi, and M. Rovere, *Confined water in the low hydration regime*, J. Chem. Phys. 117(1) (2002), pp. 369–375.
[28] P. Gallo, M.A. Ricci, and M. Rovere, *Layer analysis of the structure of water confined in vycor glass*, J. Chem. Phys. 116(1) (2002), pp. 342–346.
[29] P. Gallo, M.A. Ricci, and M. Rovere, *Supercooled confined water and the mode coupling scenario*, Phys. A 304(1–2) (2002), pp. 53–58.
[30] P. Gallo and M. Rovere, *Anomalous dynamics of confined water at low hydration*, J. Phys.: Condens. Matter 15(45) (2003), pp. 7625–7633.
[31] M. Rovere and P. Gallo, *Effects of confinement on static and dynamical properties of water*, Eur. Phys. J. E 12(1) (2003), pp. 77–81.
[32] M. Rovere and P. Gallo, *Strong layering effects and anomalous dynamical behaviour in confined water at low hydration*, J. Phys.: Condens. Matter 15(1) (2003), pp. S145–S150.
[33] L. Liu, A. Faraone, C. Mou, C.W. Yen, and S.H. Chen, *Slow dynamics of supercooled water confined in nanoporous silica materials*, J. Phys.: Condens. Matter 16(45) (2004), pp. S5403–S5436.
[34] N. Giovambattista, P.J. Rossky, and P.G. Debenedetti, *Effect of pressure on the phase behavior and structure of water confined between nanoscale hydrophobic and hydrophilic plates*, Phys. Rev. E 73 (2006), 041604-1–041604-14.
[35] A.H. Corbera, *Towards biomedical applications of nanofluidics*, *MRes in Nanomaterials*, Imperial College, London, 2003.
[36] H.J.C. Berendsen, J.R. Grigera, and T.P. Straatsma, *The missing term in effective pair potentials*, J. Phys. Chem. 91(24) (1987), pp. 6269–6271.
[37] Y.W. Tang and K.Y. Chan, *The dot and line method: a long range correction to Coulomb interaction in a cylindrical pore*, Mol. Simul. 30(1) (2004), pp. 63–70.
[38] H.S. Lee and J. Rasaiah, *Molecular dynamics simulation of ion mobility. 2. Alkali metal and halide ions using the SPC/E model for water at 25°C*, J. Phys. Chem. 100(4) (1996), pp. 1420–1425.
[39] P. Mark and L. Nisson, *Structure and dynamics of the TIP3P, SPC and SPC/E water models at 298 K*, J. Phys. Chem. A 105(43) (2001), pp. 9954–9960.
[40] W.S. Price, H. Ide, and Y. Arata, *Self-diffusion of supercooled water to 238 K using PGSE NMR diffusion measurements*, J. Phys. Chem. A 103(4) (1999), pp. 448–450.
[41] M.E. Parker and D.M. Heyes, *Molecular dynamics of stretched water: local structure and spectral signatures*, J. Chem. Phys. 108(21) (1998), pp. 9039–9049.
[42] L.L. Huang, L.Z. Zhang, Q. Shao, J. Wang, L.H. Lu, X.H. Lu, S.Y. Jiang, and W.F. Shen, *Molecular dynamics simulation study of the structural characteristics of water molecules confined in functionalized carbon nanotubes*, J. Phys. Chem. B 110(51) (2006), pp. 25761–25768.
[43] P. Raiteri, A. Laio, and M. Parrinello, *Correlations among hydrogen bonds in liquid water*, Phys. Rev. Lett. 93(8) (2004), 087801-1–087801-4.